EUROPEAN ORGANIZATION FOR NUCLEAR RESEARCH

CERN-EP-2023-069
21 April 2023

A study of the $K^+ \to \pi^0 e^+ \nu\gamma$ decay

The NA62 Collaboration *

Abstract

A sample of 1.3×10^5 $K^+ \to \pi^0 e^+ \nu\gamma$ candidates with less than 1% background was collected by the NA62 experiment at the CERN SPS in 2017–2018. Branching fraction measurements are obtained at percent relative precision in three restricted kinematic regions, improving on existing results by a factor larger than two. An asymmetry, possibly related to T-violation, is investigated with no evidence observed within the achieved precision.

To be submitted to JHEP

*email: na62eb@cern.ch
Corresponding authors: F. Brizioli (francesco.brizioli@cern.ch), D. Madigozhin (dmitry.madigozhin@cern.ch)

1 Introduction

A study of the $K^+ \to \pi^0 e^+ \nu\gamma$ decay allows a precision test of Chiral Perturbation Theory (ChPT), an effective field theory of Quantum Chromodynamics (QCD) at low energies based on the chiral symmetry properties of the QCD Lagrangian [1, 2, 3]. In this framework, the $K^+ \to \pi^0 e^+ \nu\gamma$ decay is described by inner bremsstrahlung (IB) and structure dependent (SD) processes and their interference. Calculations of the branching fraction for the $K^+ \to \pi^0 e^+ \nu\gamma$ decay at different orders of approximation of radiative effects are given in [4, 5, 6, 7].

The radiative decay $K^+ \to \pi^0 e^+ \nu\gamma$ ($K_{e3\gamma}$) is defined as a subset of the inclusive decays $K^+ \to \pi^0 e^+ \nu(\gamma)$ (K_{e3}) that requires a minimum photon energy (E_γ) and a range of angles between the positron and the radiative photon ($\theta_{e\gamma}$) in the kaon rest frame. These conditions are designed to prevent the decay amplitude from diverging in the infrared ($E_\gamma \to 0$) and collinear ($\theta_{e\gamma} \to 0$) limits.

The ratio between the branching fractions of the radiative decay $K_{e3\gamma}$ and the inclusive decay K_{e3} is expressed as:

$$R_j = \frac{\mathcal{B}(K_{e3\gamma^j})}{\mathcal{B}(K_{e3})} = \frac{\mathcal{B}(K^+ \to \pi^0 e^+ \nu\gamma \mid E_\gamma^j,\ \theta_{e\gamma}^j)}{\mathcal{B}(K^+ \to \pi^0 e^+ \nu(\gamma))}, \tag{1}$$

where $(E_\gamma^j,\ \theta_{e\gamma}^j)$ are the conditions corresponding to the kinematic regions labeled by the index j. The definitions of the three kinematic regions used in this analysis are given in Table 1, together with theoretical [6] and experimental [8, 9] R_j results. Another theoretical calculation [7] predicts the branching fraction $\mathcal{B}(K^+ \to \pi^0 e^+ \nu\gamma \mid E_\gamma > 30\ \text{MeV},\ \theta_{e\gamma} > 20^\circ) = (2.72 \pm 0.10) \times 10^{-4}$, that is converted to R_2 using the K_{e3} branching fraction [10]: $R_2 = (0.54 \pm 0.02) \times 10^{-2}$.

Table 1: Definition of kinematic regions, R_j expectations from ChPT $\mathcal{O}(p^6)$ calculations [6] and measurements from ISTRA+ [8] and OKA [9] experiments, with statistical and systematic uncertainties quoted separately.

	$E_\gamma^j,\ \theta_{e\gamma}^j$	ChPT	ISTRA+	OKA
$R_1 \times 10^2$	$E_\gamma > 10$ MeV, $\theta_{e\gamma} > 10^\circ$	1.804 ± 0.021	$1.81 \pm 0.03 \pm 0.07$	$1.990 \pm 0.017 \pm 0.021$
$R_2 \times 10^2$	$E_\gamma > 30$ MeV, $\theta_{e\gamma} > 20^\circ$	0.640 ± 0.008	$0.63 \pm 0.02 \pm 0.03$	$0.587 \pm 0.010 \pm 0.015$
$R_3 \times 10^2$	$E_\gamma > 10$ MeV, $0.6 < \cos\theta_{e\gamma} < 0.9$	0.559 ± 0.006	$0.47 \pm 0.02 \pm 0.03$	$0.532 \pm 0.010 \pm 0.012$

The amplitude of the $K_{e3\gamma}$ decay is sensitive to T-violating contributions, which can be studied with the T-odd observable ξ and the corresponding T-asymmetry A_ξ, defined as:

$$\xi = \frac{\vec{p_\gamma} \cdot (\vec{p_e} \times \vec{p_\pi})}{(M_K \cdot c)^3},\ A_\xi = \frac{N_+ - N_-}{N_+ + N_-}, \tag{2}$$

where $\vec{p}$ is the three-momentum of each particle in the kaon rest frame, M_K is the charged kaon mass [10] and N_+ (N_-) is the number of events with positive (negative) values of ξ.

Theoretical calculations of A_ξ, within the Standard Model (SM) and beyond [5, 7, 11, 12], predict values in the range $[-10^{-4}, -10^{-5}]$. Non-zero values of A_ξ in the SM originate from one-loop electromagnetic corrections. The uncertainty of the most precise published A_ξ measurement [13] is two orders of magnitude larger than theoretical expectation.

2 The NA62 experiment at CERN

The beam and detector of the NA62 experiment at the CERN SPS, designed to study the $K^+ \to \pi^+ \nu\bar{\nu}$ decay [14], are described in [15]. A schematic view of the NA62 setup is presented in Figure 1.

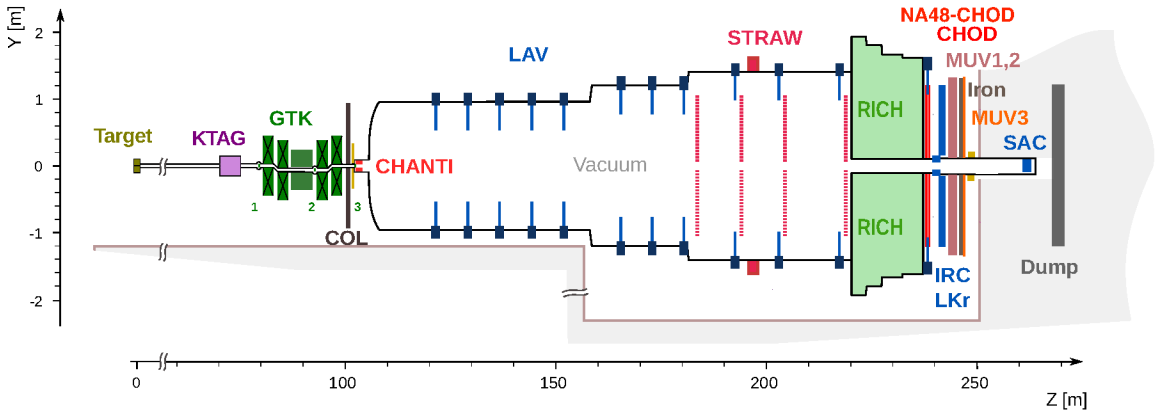

Figure 1: Schematic side view of the NA62 beam line and detector.

A 400 GeV/c proton beam extracted from the SPS impinges on the kaon production target in spills of three seconds effective duration. The target position defines the origin of the NA62 reference system: the beam travels along the Z axis in the positive direction (downstream), the Y axis points vertically up, and the X axis is horizontal and directed to form a right-handed coordinate system. Typical intensities during data taking range from 1.7 to 1.9 $\times 10^{12}$ protons per spill. The resulting unseparated secondary hadron beam of positively charged particles contains 70% π^+, 23% protons, 6% K^+, with a central beam momentum of 75 GeV/c and 1% rms momentum bite.

Beam kaons are tagged with a time resolution of 70 ps by a differential Cherenkov counter (KTAG), with a 5 m long vessel containing nitrogen gas at 1.75 bar pressure, which acts as the radiator. Beam particle positions, momenta and times (to better than 100 ps resolution) are measured by a silicon pixel spectrometer consisting of three stations (GTK1,2,3) and four dipole magnets. The typical beam particle rate at the third GTK station is about 450 MHz.

The last station is immediately preceded by a 1.2 m thick steel collimator (COL) with a 76 $\times$ 40 mm^2 central aperture and 1.7 $\times$ 1.8 m^2 outer dimensions, to absorb hadrons from upstream K^+ decays. A variable aperture collimator of about 0.15 $\times$ 0.15 m^2 outer dimensions was used up to early 2018.

The GTK3 station marks the beginning of a 117 m long vacuum tank. In this analysis, a 60 m long fiducial volume (FV), in which 10% of the kaons decay, is defined starting 7.6 m downstream of GTK3. The beam has a rectangular transverse profile of 52 $\times$ 24 mm^2 and an angular spread of 0.11 mrad (rms) at the FV entrance.

The time, momentum and direction of charged particles produced by kaon decays are measured by a magnetic spectrometer (STRAW). The STRAW, comprised of two pairs of straw chambers on either side of a dipole magnet, measures momenta with a resolution $\sigma_p/p = (0.30 \oplus 0.005 \cdot p)\%$, where the momentum p is expressed in GeV/c. The ring-imaging Cherenkov counter (RICH), filled with neon at atmospheric pressure, tags the decay particles with a timing precision better than 100 ps and provides particle identification. The CHOD, a matrix of tiles read out by Silicon photomultipliers, and the NA48-CHOD, composed of two orthogonal planes of scintillating slabs, are used for triggering and timing, providing a time measurement with 200 ps resolution.

Six stations of plastic scintillator bars (CHANTI) detect, with 99% efficiency and 1 ns time resolution, extra activity, including inelastic interactions in GTK3. Twelve stations of ring-shaped electromagnetic calorimeters (LAV), made of lead-glass blocks, are located inside and downstream of the vacuum tank to achieve full acceptance for photons emitted by K^+ decays in

the FV at polar angles between 10 and 50 mrad. A 27 radiation-length thick, quasi-homogeneous liquid krypton electromagnetic calorimeter (LKr) detects photons from K^+ decays emitted at angles between 1 and 10 mrad. Its energy resolution is $\sigma(E)/E = (4.8/\sqrt{E} \oplus 11/E \oplus 0.9)\%$, where the energy E is expressed in GeV. Its spatial and time resolutions are 1 mm and between 0.5 and 1 ns, respectively, depending on the amount and source of energy released. The LKr also complements the RICH particle identification. Two hadronic iron/scintillator-strip sampling calorimeters (MUV1,2) and an array of scintillator tiles located behind 80 cm of iron (MUV3) supplement the pion/muon identification system. MUV3 has a time resolution of 400 ps. A lead/scintillator shashlik calorimeter (IRC) located in front of the LKr and a detector based on the same principle (SAC) placed on the Z axis at the downstream end of the apparatus, ensure the detection of photons down to zero degrees in the forward direction. The IRC and SAC detectors compose the Small Angle Veto system (SAV). LAV, LKr and SAV make the photon veto system almost hermetic for photons emitted by kaon decays in the FV.

A two-level trigger system is used, with a hardware low level trigger, L0, and a software high level trigger, L1 [16, 17]. Auxiliary trigger lines are operated concurrently with the main trigger line that is dedicated to the $K^+ \to \pi^+\nu\bar{\nu}$ decay. This analysis uses the *non-μ* and the *control* trigger lines described below.

- The *non-μ* line requires signals in the RICH and CHOD detectors at L0, compatible with the presence of at least one charged particle in the final state, and no signal in the MUV3 detector in time coincidence. A signal in the KTAG detector is required at L1, compatible with the presence of a charged kaon. In a fraction of the dataset, a track reconstructed by the STRAW is also required at L1. This trigger line is downscaled by a factor of 200.
- The *control* line requires the presence of signal in the NA48-CHOD detector at L0, compatible with the presence of a charged particle in the final state. No requirements are applied at L1. This trigger line is downscaled by a factor of 400.

This analysis exploits the data collected by the NA62 experiment in 2017–2018. Monte Carlo (MC) simulations of particle interactions with the detector and its response are performed using a software package based on the Geant4 toolkit [18].

3 Event selection

Signal ($K_{e3\gamma}$) and normalization (K_{e3}) events share the same selection criteria, except for the requirement of an additional photon in the signal sample. This ensures a first-order cancellation of several systematic effects in the R_j measurements.

3.1 Common selection criteria

A positively charged track is required to be reconstructed in the STRAW with momentum in the range 10–60 GeV/c. Its extrapolated positions in the CHOD, NA48-CHOD, RICH and LKr front planes should be within the respective geometrical acceptances. A spatial association of signals in these detectors is required, together with time association within 2 ns. Positron identification is achieved by applying conditions on the reconstructed RICH ring radius and on the ratio of the energy of the LKr cluster associated with the track and the measured track momentum.

The beam track is reconstructed in the GTK and identified as a kaon by an associated signal in KTAG within 2 ns. The positron and kaon tracks are matched taking into account both space (closest distance of approach smaller than 10 mm) and time ($\pm$0.5 ns) coincidence. The mid-point of the segment at the closest distance of approach of the two tracks defines the kaon decay vertex, which is required to be within the FV.

The *event time* (T_{event}) is defined as the weighted average of the times measured by the KTAG, GTK, RICH and NA48-CHOD detectors, taking into account the resolutions of each detector, and is required to be within 10 ns of the trigger time.

The two photons from $\pi^0 \to \gamma\gamma$ decay are identified by selecting two LKr clusters, not associated to any track, with energy above 4 GeV and within 3 ns of T_{event}. The four-momentum of each photon is reconstructed using the energy and position of the cluster, assuming that the photon is produced at the kaon decay vertex. The di-photon mass is required to be compatible with the π^0 mass. The π^0 four-momentum is defined as the sum of the four-momenta of the two photons.

The *LKr time* (T_{LKr}) is defined as the average of the times of the three LKr clusters associated with the positron and the photon pair forming the π^0.

Events with activity in the LAV and SAV within 15 ns of T_{event} are rejected to suppress background events coming mainly from $K^+ \to \pi^0\pi^0 e^+\nu$ decays. Events with signals in MUV3 within 15 ns of T_{event} are rejected to suppress background events with muons in the final state.

3.2 Specific selection criteria

The following exclusive criteria are applied to select signal and normalization candidates.

Normalization selection. The squared missing mass $m^2_{\text{miss}}(K_{e3}) = (P_K - P_e - P_{\pi^0})^2$ must satisfy $|m^2_{\text{miss}}(K_{e3})| < 11000$ MeV$^2/c^4$, where P_K, P_e and P_{π^0} are the reconstructed kaon, positron and π^0 four-momenta. Events are rejected if a fourth LKr cluster is detected with energy above 2 GeV and within 15 ns of T_{LKr}.

Signal selection. A fourth isolated cluster with energy above 4 GeV and time T_γ within 3 ns of T_{LKr} must be present. It is identified as the radiative photon and attached to the kaon decay vertex. Events are rejected if a fifth LKr cluster is detected with energy above 2 GeV and within 15 ns of T_{LKr}. This condition further suppresses the $K^+ \to \pi^0\pi^0 e^+\nu$ background events.

The squared missing mass $m^2_{\text{miss}}(K_{e3\gamma}) = (P_K - P_e - P_{\pi^0} - P_\gamma)^2$ must satisfy $|m^2_{\text{miss}}(K_{e3\gamma})| < 11000$ MeV$^2/c^4$ and $m^2_{\text{miss}}(K_{e3}) > 5000$ MeV$^2/c^4$, where P_γ is the reconstructed four-momentum of the radiative photon.

The background from K_{e3} events, with a bremsstrahlung photon emitted by positron interactions in the detector material, is suppressed by requiring a minimum distance between the radiative photon cluster and the intersection of the positron line of flight at the vertex with the LKr plane.

Selection conditions on E_γ and $\theta_{e\gamma}$ are applied according to the three kinematic region definitions, to obtain the signal sample S_1 and its subsets S_2 and S_3.

4 Signal rate measurement

The ratios R_j, defined in eq. (1), are measured as:

$$R_j = \frac{\mathcal{B}(K_{e3\gamma^j})}{\mathcal{B}(K_{e3})} = \frac{N^{\text{obs}}_{Ke3\gamma^j} - N^{\text{bkg}}_{Ke3\gamma^j}}{N^{\text{obs}}_{Ke3} - N^{\text{bkg}}_{Ke3}} \cdot \frac{A_{Ke3}}{A_{Ke3\gamma^j}} \cdot \frac{\epsilon^{\text{trig}}_{Ke3}}{\epsilon^{\text{trig}}_{Ke3\gamma^j}}. \tag{3}$$

Here, $N^{\text{obs}}_{Ke3\gamma^j}$ and $N^{\text{bkg}}_{Ke3\gamma^j}$ are the numbers of observed signal candidates and expected background events in the signal samples, and $A_{Ke3\gamma^j}$ and $\epsilon^{\text{trig}}_{Ke3\gamma^j}$ are the related acceptances and the trigger efficiencies. Similarly, N^{obs}_{Ke3} and N^{bkg}_{Ke3} are the numbers of observed normalization

candidates and expected background events in the normalization sample, and A_{Ke3} and $\epsilon^{\rm trig}_{Ke3}$ are the related acceptance and the trigger efficiency.

The signal selection acceptances are defined with respect to the corresponding kinematic regions, while the normalization selection acceptance is defined with respect to the full phase-space. They are evaluated using simulations. A ChPT $\mathcal{O}(p^6)$ description of the signal decay is used [6]. The normalization decay description includes only the IB component [19]. The resulting acceptances are reported in Table 2 together with the numbers of selected candidates.

The trigger conditions are replicated in the selections and are only related to the presence of charged particles. The *non-μ* and *control* trigger lines yield independent data samples. Each is used to evaluate the efficiency of the other. The result is that the ratios $\epsilon^{\rm trig}_{Ke3}/\epsilon^{\rm trig}_{Ke3\gamma^j}$ are consistent with unity within 0.1%.

4.1 Background estimation

The only sizeable background in the normalization sample comes from $K^+ \to \pi^+\pi^0$ decays with the π^+ misidentified as e^+. The main background in the signal sample comes from K_{e3} and $K^+ \to \pi^+\pi^0$ decays (with π^+ misidentification in the latter case) with an extra cluster due to accidental activity in the LKr that mimics the radiative photon (accidental background). The accidental background is measured from the data (Figure 2), using the side-bands $6 < |T_\gamma - T_{\rm LKr}| < 9$ ns and assuming a flat $T_\gamma - T_{\rm LKr}$ distribution. This assumption is validated and the systematic uncertainty is evaluated using the validation side-bands $9 < |T_\gamma - T_{\rm LKr}| < 12$ ns. An additional contribution to the background in the signal sample stems from $K^+ \to \pi^0\pi^0 e^+\nu$ decays with a photon from the $\pi^0 \to \gamma\gamma$ decay not detected. Contributions from other potential background channels, *e.g.* $K^+ \to \pi^+\pi^0\pi^0$, are found to be negligible.

All the background contributions, except for the accidental background, are estimated with simulations. The values of the branching fractions of the normalization and the background channels are taken from [10]. Backgrounds are summarised in Table 2. The distributions of $m^2_{\rm miss}(K_{e3})$ for the selected normalization events, and of $m^2_{\rm miss}(K_{e3\gamma})$ for the selected signal events, are shown in Figure 3 for the data, estimated backgrounds and simulated signal and normalization.

Table 2: Numbers of selected candidates, acceptances, background estimates and fractional background for the normalization and the three signal samples. The $K^+ \to \pi^+\pi^0$ background in the signal samples is included in the accidental background. Upper limits at 68% CL are quoted when no simulated events satisfy the selection.

	Normalization	S_1	S_2	S_3
Selected candidates	6.6420×10^7	1.2966×10^5	0.5359×10^5	0.3909×10^5
Acceptance	$(3.842 \pm 0.002)\%$	$(0.444 \pm 0.001)\%$	$(0.514 \pm 0.002)\%$	$(0.432 \pm 0.002)\%$
Accidental	—	$(4.9 \pm 0.2 \pm 1.3) \times 10^2$	$(2.3 \pm 0.2 \pm 0.3) \times 10^2$	$(1.1 \pm 0.1 \pm 0.5) \times 10^2$
$K^+ \to \pi^0\pi^0 e^+\nu$	—	$(1.1 \pm 1.1) \times 10^2$	$(1.1 \pm 1.1) \times 10^2$	$(0.1 \pm 0.1) \times 10^2$
$K^+ \to \pi^+\pi^0\pi^0$	—	< 20	< 20	< 20
$K^+ \to \pi^+\pi^0$	$(1.0 \pm 1.0) \times 10^4$	—	—	—
Total background	$(1.0 \pm 1.0) \times 10^4$	$(6.0 \pm 1.8) \times 10^2$	$(3.4 \pm 1.2) \times 10^2$	$(1.2 \pm 0.6) \times 10^2$
Fractional background	1.6×10^{-4}	0.46×10^{-2}	0.64×10^{-2}	0.29×10^{-2}

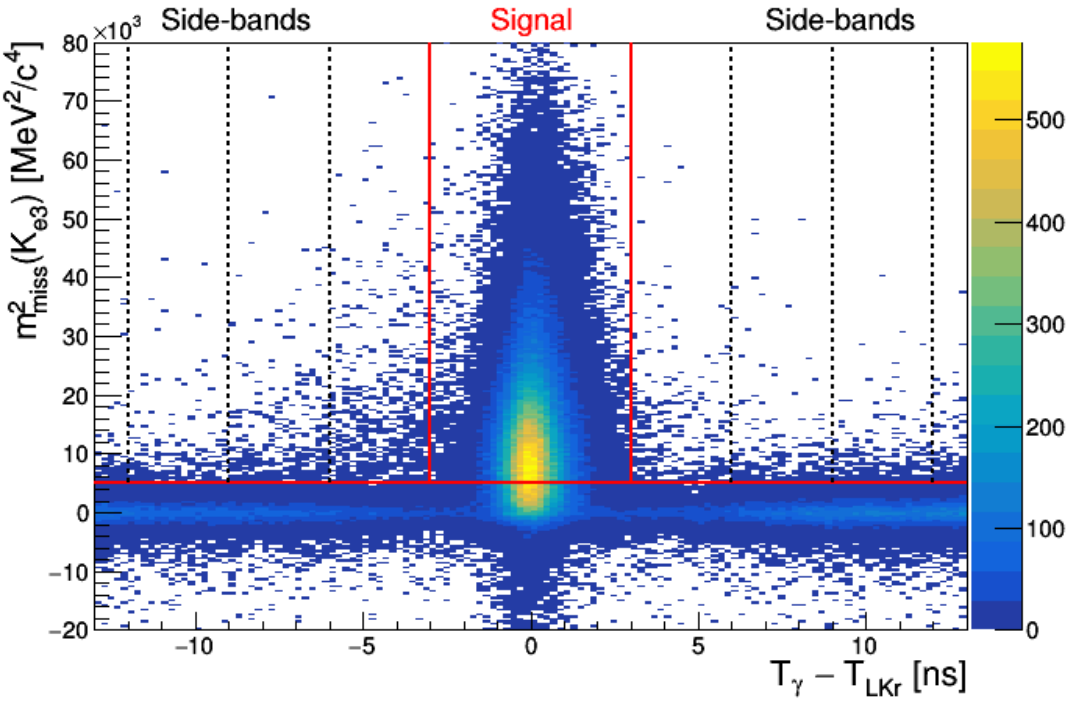

Figure 2: Reconstructed $m^2_{\rm miss}(K_{e3})$ of signal candidates as a function of the time difference $T_\gamma - T_{\rm LKr}$. The $m^2_{\rm miss}(K_{e3})$ condition is shown (red horizontal line), together with the signal selection time window (red vertical lines) and the side-bands (black dashed vertical lines).

4.2 LKr response correction

The signal selection acceptance is sensitive to the precision of the low-energy photon measurement in the LKr due to the steeply falling radiative photon energy spectrum. The minimum radiative photon energy considered in the analysis is 4 GeV, while the standard LKr fine calibration procedures exploit $\pi^0 \to \gamma\gamma$ and $\pi^0 \to \gamma e^+ e^-$ decays, and provide optimal precision in the 10–30 GeV energy range. A dedicated procedure is therefore employed to modify the LKr response in the simulated samples and estimate the corresponding systematic uncertainty. The procedure is based on improving the agreement between data and simulated distributions in the most relevant variables, $m^2_{\rm miss}(K_{e3})$ and $m^2_{\rm miss}(K_{e3\gamma})$. The LKr response modification includes a constant energy scale factor, an energy-dependent factor, and an additional stochastic smearing of the measured energy.

The correction factors $f_j^{\rm LKr}$ are defined as the ratios of the corrected $A_{Ke3}/A_{Ke3\gamma^j}$ values to the original values. The systematic uncertainties in $f_j^{\rm LKr}$ are evaluated as quadratic sums of three terms: the maximum deviations of $f_j^{\rm LKr}$ from their central values obtained by varying the modification parameters within their uncertainties; half of the size of the overall correction; and half of the maximum variation of $f_j^{\rm LKr}$ obtained using alternative LKr fine calibration procedures based on different methods of π^0 mass reconstruction. The correction factors and their uncertainties are listed in Table 3. The acceptance ratios $A_{Ke3}/A_{Ke3\gamma^j}$ (Table 2) must be multiplied by $f_j^{\rm LKr}$.

4.3 Photon veto correction

The signal and normalization MC generators, used to evaluate acceptance, simulate exactly one radiative photon per event. Both the normalization and signal selections forbid the presence of

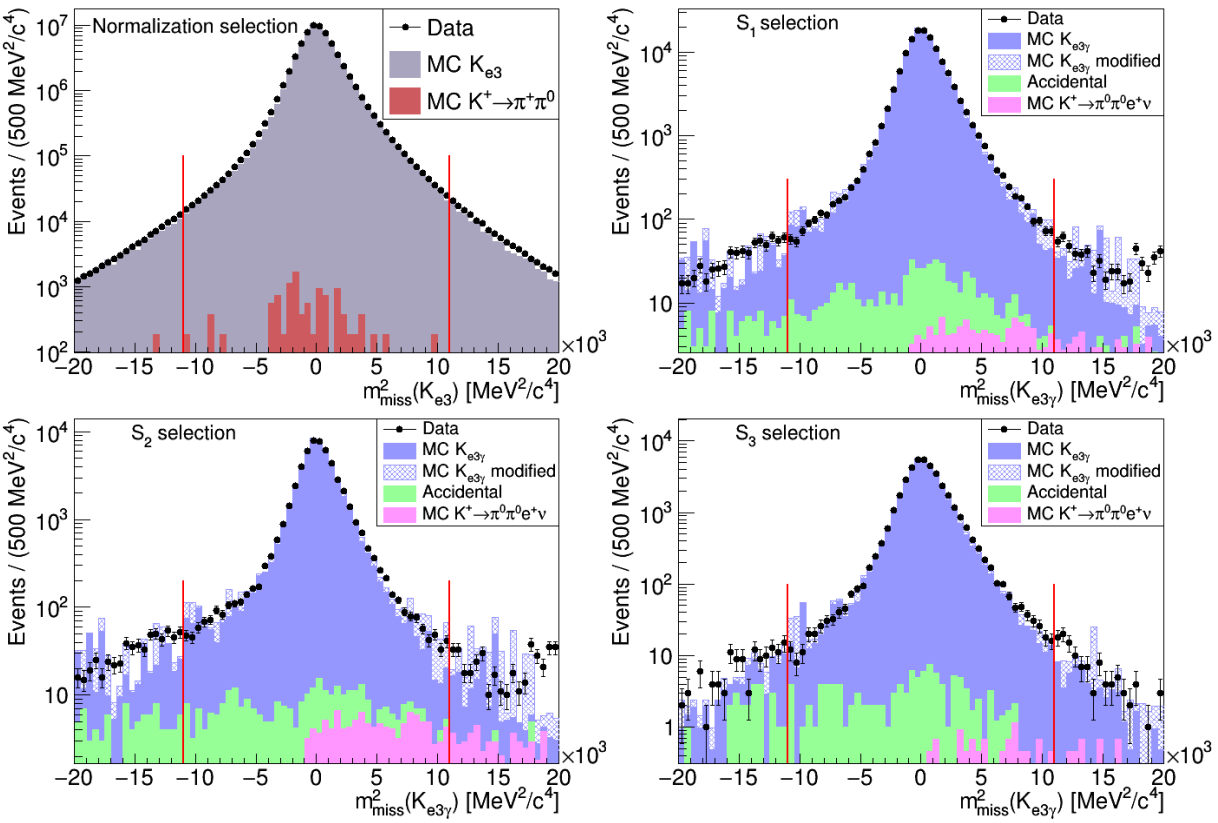

Figure 3: Top left: $m^2_{\rm miss}(K_{e3})$ distribution of the normalization sample for data (points) and expected signal and background (histograms). Other panels: $m^2_{\rm miss}(K_{e3\gamma})$ distributions of the three signal samples for data (points) and expected signal and backgrounds (histograms); the "$K_{e3\gamma}$ modified" histogram represents the distribution after modification of the LKr response in the simulation (Section 4.2). The red lines correspond to the selection conditions.

in-time extra clusters in the LKr with energy above 2 GeV, as well as in-time signals in the LAV and SAV. The radiative photon contributes to the photon veto simulation in the normalization case, but not in the signal case where it is included in the signal event reconstruction. Additional radiative photons are not generated in the simulated samples, leading to a systematic underestimation of the acceptance ratios $A_{Ke3}/A_{Ke3\gamma^j}$. However, special signal and normalization MC samples with multiple radiative photons are generated using the PHOTOS program [20], providing a less accurate description of the radiative effects than the standard MC samples and therefore used only to evaluate the photon veto effects. The resulting correction factors $f_j^{\rm PV}$ are reported in Table 3. The acceptance ratios $A_{Ke3}/A_{Ke3\gamma^j}$ (Table 2) must be multiplied by $f_j^{\rm PV}$.

The uncertainties in $f_j^{\rm PV}$ include MC statistical uncertainties, variations of the simulated LAV and SAV efficiencies when replaced by the measured energy-dependent values [21], and the variation of the LKr veto efficiency with the LKr response tuning. The deviation of $f_j^{\rm PV}$ from unity is dominated by the LKr contribution, while the uncertainties in $f_j^{\rm PV}$ are dominated by the LAV contributions.

4.4 Theoretical model uncertainty

The theoretical model used in the MC simulation of the $K_{e3\gamma}$ decay, based on ChPT $\mathcal{O}(p^6)$, results in a 30% relative uncertainty in the contribution to the decay width arising from the SD component and its interference with the IB component [6]. The acceptances evaluated with

Table 3: Correction factors to the acceptance ratios $A_{Ke3}/A_{Ke3\gamma^j}$ from LKr response modelling ($f_j^{\rm LKr}$) and photon veto ($f_j^{\rm PV}$), for the three signal samples.

	S_1	S_2	S_3
$f_j^{\rm LKr}$	0.9967 ± 0.0038	0.9941 ± 0.0047	0.9996 ± 0.0039
$f_j^{\rm PV}$	1.0234 ± 0.0028	1.0243 ± 0.0036	1.0216 ± 0.0031

the signal MC sample are compared with those evaluated with the K_{e3} MC sample generated including only the IB component of the radiative effects [19], and 30% of their relative difference is considered as a relative systematic uncertainty in $A_{Ke3\gamma^j}$.

4.5 Results

The measured R_j values are:

$$R_1 \times 10^2 = 1.715 \pm 0.005_{\rm stat} \pm 0.010_{\rm syst} = 1.715 \pm 0.011,$$
$$R_2 \times 10^2 = 0.609 \pm 0.003_{\rm stat} \pm 0.006_{\rm syst} = 0.609 \pm 0.006,$$
$$R_3 \times 10^2 = 0.533 \pm 0.003_{\rm stat} \pm 0.004_{\rm syst} = 0.533 \pm 0.004.$$

The error budgets are given in Table 4. The statistical uncertainties quoted arise from the numbers of observed candidates in the data, while all other contributions are considered as systematic uncertainties. The stability of the results is checked by splitting the data sample into subsamples, and by varying the selection conditions, with no evidence for residual systematic effects.

Table 4: Relative uncertainties in the R_j measurements.

	$\delta R_1/R_1$	$\delta R_2/R_2$	$\delta R_3/R_3$
Statistical	0.3%	0.4%	0.5%
Limited MC sample size	0.2%	0.4%	0.4%
Background estimation	0.1%	0.2%	0.1%
LKr response modelling	0.4%	0.5%	0.4%
Photon veto correction	0.3%	0.4%	0.3%
Theoretical model	0.1%	0.5%	0.1%
Total systematic	0.6%	0.9%	0.7%
Total	0.7%	1.0%	0.8%

The measured values are 5% smaller than the ChPT $\mathcal{O}(p^6)$ calculations [6], with a disagreement at the level of three standard deviations. The smaller and less precise value of R_2 given in [7] is also different from the measurement at the level of three standard deviations.

5 T-asymmetry measurement

The T-asymmetry A_ξ is measured using the $K_{e3\gamma}$ samples selected for the R_j measurements. The distributions of the ξ observable are shown in Figure 4, for data and simulation.

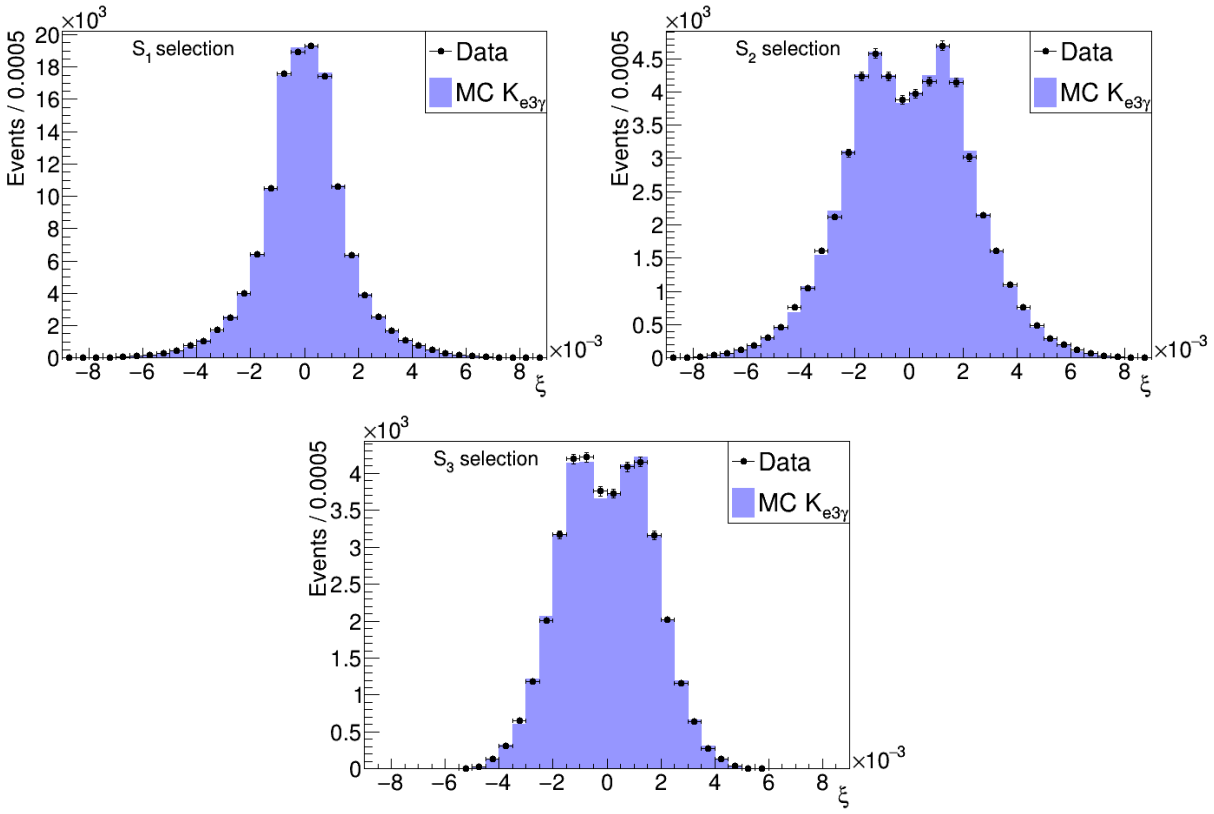

Figure 4: Distributions of the reconstructed ξ observable for the three signal samples for data (points) and simulations (histograms).

For each selected signal sample, a raw asymmetry measurement $A_\xi^{\rm Data}$ is obtained using eq. (2). An offset $A_\xi^{\rm MC}$, possibly introduced by the detector and the selection, is measured by comparing the reconstructed and generated asymmetry values in the $K_{e3\gamma}$ simulated sample. The generated asymmetry value is checked to be zero within a $\mathcal{O}(10^{-4})$ precision in the three $K_{e3\gamma}$ kinematic regions considered, in agreement with the ChPT $\mathcal{O}(p^6)$ calculations [12]. The final measurement is obtained as $A_\xi^{\rm NA62} = A_\xi^{\rm Data} - A_\xi^{\rm MC}$. The uncertainty in $A_\xi^{\rm MC}$, due to the limited statistics of the $K_{e3\gamma}$ simulated sample, is propagated as a systematic uncertainty. No statistically significant asymmetry is observed, as reported in Table 5.

Table 5: Results of the A_ξ measurements for the three signal samples. The measurements by the OKA experiment [13], $A_\xi^{\rm OKA}$, are also reported for comparison. The sign of the OKA results is changed for consistency with eq. (2).

		S_1	S_2	S_3
$A_\xi^{\rm Data}$	$\times 10^3$	$1.9 \pm 2.8_{\rm stat}$	$1.3 \pm 4.3_{\rm stat}$	$-6.2 \pm 5.1_{\rm stat}$
$A_\xi^{\rm MC}$	$\times 10^3$	$3.1 \pm 1.9_{\rm syst}$	$4.8 \pm 3.0_{\rm syst}$	$3.0 \pm 3.5_{\rm syst}$
$A_\xi^{\rm NA62}$	$\times 10^3$	$-1.2 \pm 2.8_{\rm stat} \pm 1.9_{\rm syst}$	$-3.4 \pm 4.3_{\rm stat} \pm 3.0_{\rm syst}$	$-9.1 \pm 5.1_{\rm stat} \pm 3.5_{\rm syst}$
$A_\xi^{\rm OKA}$	$\times 10^3$	$-0.1 \pm 3.9_{\rm stat} \pm 1.7_{\rm syst}$	$7.0 \pm 8.1_{\rm stat} \pm 1.5_{\rm syst}$	$-4.4 \pm 7.9_{\rm stat} \pm 1.9_{\rm syst}$

6 Summary

Measurements of the ratio of the $K^+ \to \pi^0 e^+ \nu\gamma$ to $K^+ \to \pi^0 e^+ \nu(\gamma)$ branching fractions, together with measurements of the T-violating asymmetry in the $K^+ \to \pi^0 e^+ \nu\gamma$ decay, are performed in three kinematic regions using data collected by the NA62 experiment at CERN in 2017–2018.

The measured ratios, $R_1 = (1.715 \pm 0.011) \times 10^{-2}$, $R_2 = (0.609 \pm 0.006) \times 10^{-2}$, $R_3 = (0.533 \pm 0.004) \times 10^{-2}$, are at least a factor of two more precise than previous measurements. The relative uncertainties do not exceed 1%, matching the precision of the most precise theoretical calculations.

The T-asymmetry measurements performed at an improved precision are compatible with no asymmetry in the three kinematic regions considered. Their uncertainties remain two orders of magnitude larger than the theoretical expectations.

Acknowledgements

It is a pleasure to express our appreciation to the staff of the CERN laboratory and the technical staff of the participating laboratories and universities for their efforts in the operation of the experiment and data processing.

The cost of the experiment and its auxiliary systems was supported by the funding agencies of the Collaboration Institutes. We are particularly indebted to: F.R.S.-FNRS (Fonds de la Recherche Scientifique - FNRS), under Grants No. 4.4512.10, 1.B.258.20, Belgium; CECI (Consortium des Equipements de Calcul Intensif), funded by the Fonds de la Recherche Scientifique de Belgique (F.R.S.-FNRS) under Grant No. 2.5020.11 and by the Walloon Region, Belgium; NSERC (Natural Sciences and Engineering Research Council), funding SAPPJ-2018-0017, Canada; MEYS (Ministry of Education, Youth and Sports) funding LM 2018104, Czech Republic; BMBF (Bundesministerium für Bildung und Forschung) contracts 05H12UM5, 05H15UMCNA and 05H18UMCNA, Germany; INFN (Istituto Nazionale di Fisica Nucleare), Italy; MIUR (Ministero dell'Istruzione, dell'Università e della Ricerca), Italy; CONACyT (Consejo Nacional de Ciencia y Tecnología), Mexico; IFA (Institute of Atomic Physics) Romanian CERN-RO No. 1/16.03.2016 and Nucleus Programme PN 19 06 01 04, Romania; MESRS (Ministry of Education, Science, Research and Sport), Slovakia; CERN (European Organization for Nuclear Research), Switzerland; STFC (Science and Technology Facilities Council), United Kingdom; NSF (National Science Foundation) Award Numbers 1506088 and 1806430, U.S.A.; ERC (European Research Council) "UniversaLepto" advanced grant 268062, "KaonLepton" starting grant 336581, Europe.

Individuals have received support from: Charles University Research Center (UNCE/SCI/013), Czech Republic; Ministero dell'Istruzione, dell'Università e della Ricerca (MIUR "Futuro in ricerca 2012" grant RBFR12JF2Z, Project GAP), Italy; the Royal Society (grants UF100308, UF0758946), United Kingdom; STFC (Rutherford fellowships ST/J00412X/1, ST/M005798/1), United Kingdom; ERC (grants 268062, 336581 and starting grant 802836 "AxScale"); EU Horizon 2020 (Marie Skłodowska-Curie grants 701386, 754496, 842407, 893101, 101023808).

References

[1] S. Weinberg, *Phenomenological Lagrangians*, Physica A: Statistical Mechanics and its Applications **96** (1979) 327.

[2] J. Gasser, H. Leutwyler, *Chiral perturbation theory to one loop*, Annals of Physics **158** (1984) 142.

[3] J. Gasser, H. Leutwyler, *Chiral perturbation theory: Expansions in the mass of the strange quark*, Nucl. Phys. B **250** (1985) 465.

[4] J. Bijnens, G. Ecker, J. Gasser, *Radiative semileptonic kaon decays*, Nucl. Phys. B **396** (1993) 81.

[5] V. V. Braguta, A. A. Likhoded, A. E. Chalov, *T-odd correlation in the $K_{l3\gamma}$ decay*, Phys. Rev. D **65** (2002) 054038.

[6] B. Kubis, E. H. Muller, J. Gasser, M. Schmid, *Aspects of radiative K^+_{e3} decays*, Eur. Phys. J. C **50** (2007) 557.

[7] I. B. Khriplovich, A. S. Rudenko, *$K^+_{l3\gamma}$ decays revisited: branching ratios and T-odd momenta correlations*, Phys. Atom. Nucl. **74** (2011) 1214.

[8] S. A. Akimenko et al. (ISTRA+ Collaboration), *Study of $K^- \to \pi^0 e^- \bar{\nu}_e \gamma$ Decay with ISTRA+ Setup*, Phys. Atom. Nucl. **70** (2007) 702.

[9] A. Y. Polyarush et al. (OKA Collaboration), *Study of $K^+ \to \pi^0 e^+ \nu\gamma$ decay with OKA setup*, Eur. Phys. J. C **81** (2021) 161.

[10] R. L. Workman et al. (Particle Data Group), *Review of Particle Physics*, Prog. Theor. Exp. Phys. **2022** (2022) 083C01.

[11] V. V. Braguta, A. A. Likhoded, A. E. Chalov, *T-odd correlation in the $K^+ \to \pi l \nu\gamma$ decays beyond the standard model*, Phys. Rev. D **68** (2003) 094008.

[12] E. H. Muller, B. Kubis, Ulf-G. Meissner, *T-odd correlations in radiative K^+_{l3} decays and chiral perturbation theory*, Eur. Phys. J. C **48** (2006) 427.

[13] A. Y. Polyarush et al. (OKA Collaboration), *Measurement of the T-Odd Correlation in the $K^+ \to \pi^0 e^+ \nu_e \gamma$ Radiative Decay at the OKA Setup*, JETP Lett. **116** (2022) 608.

[14] E. Cortina Gil et al. (NA62 Collaboration), *Measurement of the very rare $K^+ \to \pi^+ \nu\bar{\nu}$ decay*, JHEP **06** (2021) 093.

[15] E. Cortina Gil et al. (NA62 Collaboration), *The beam and detector of the NA62 experiment at CERN*, JINST **12** (2017) P05025.

[16] R. Ammendola et al., *The integrated low-level trigger and readout system of the CERN NA62 experiment*, Nucl. Instrum. Meth. A **929** (2019) 1.

[17] E. Cortina Gil et al. (NA62 Collaboration), *Performance of the NA62 trigger system*, JHEP **03** (2023) 122.

[18] J. Allison et al., *Recent developments in Geant4*, Nucl. Instrum. Meth. A **835** (2016) 186.

[19] C. Gatti, *Monte Carlo simulation for radiative kaon decays*, Eur. Phys. J. C **45** (2006) 417.

[20] E. Barberio, Z. Was, *PHOTOS - a universal Monte Carlo for QED radiative corrections: version 2.0*, Computer Physics Communications **79** (1994) 291.

[21] E. Cortina Gil et al. (NA62 Collaboration), *Search for π^0 decays to invisible particles*, JHEP **02** (2021) 201.

The NA62 Collaboration

Université Catholique de Louvain, Louvain-La-Neuve, Belgium
E. Cortina Gil, A. Kleimenova [1], E. Minucci [2], S. Padolski [3], P. Petrov, A. Shaikhiev [4], R. Volpe [5]

TRIUMF, Vancouver, British Columbia, Canada
T. Numao, Y. Petrov, B. Velghe, V. W. S. Wong

University of British Columbia, Vancouver, British Columbia, Canada
D. Bryman [6], J. Fu

Charles University, Prague, Czech Republic
Z. Hives, T. Husek [7], J. Jerhot [8], K. Kampf, M. Zamkovsky [9]

Institut für Physik and PRISMA Cluster of Excellence, Universität Mainz, Mainz, Germany
A.T. Akmete, R. Aliberti [10], G. Khoriauli [11], J. Kunze, D. Lomidze [12], L. Peruzzo, M. Vormstein, R. Wanke

Dipartimento di Fisica e Scienze della Terra dell'Università e INFN, Sezione di Ferrara, Ferrara, Italy
P. Dalpiaz, M. Fiorini, I. Neri, A. Norton [13], F. Petrucci, M. Soldani, H. Wahl [14]

INFN, Sezione di Ferrara, Ferrara, Italy
L. Bandiera, A. Cotta Ramusino, A. Gianoli, A. Mazzolari, M. Romagnoni, A. Sytov

Dipartimento di Fisica e Astronomia dell'Università e INFN, Sezione di Firenze, Sesto Fiorentino, Italy
E. Iacopini, G. Latino, M. Lenti, P. Lo Chiatto, I. Panichi, A. Parenti

INFN, Sezione di Firenze, Sesto Fiorentino, Italy
A. Bizzeti [15], F. Bucci

Laboratori Nazionali di Frascati, Frascati, Italy
A. Antonelli, G. Georgiev [16], V. Kozhuharov [16], G. Lanfranchi, S. Martellotti, M. Moulson, T. Spadaro, G. Tinti

Dipartimento di Fisica "Ettore Pancini" e INFN, Sezione di Napoli, Napoli, Italy
F. Ambrosino, T. Capussela, M. Corvino, M. D'Errico, D. Di Filippo, R. Fiorenza [17], R. Giordano, P. Massarotti, M. Mirra, M. Napolitano, G. Saracino

Dipartimento di Fisica e Geologia dell'Università e INFN, Sezione di Perugia, Perugia, Italy
G. Anzivino, F. Brizioli [*, 9], E. Imbergamo, R. Lollini, R. Piandani [18], C. Santoni

INFN, Sezione di Perugia, Perugia, Italy
M. Barbanera, P. Cenci, B. Checcucci, P. Lubrano, M. Lupi [19], M. Pepe, M. Piccini

Dipartimento di Fisica dell'Università e INFN, Sezione di Pisa, Pisa, Italy
F. Costantini, L. Di Lella [14], N. Doble [14], M. Giorgi, S. Giudici, G. Lamanna, E. Lari, E. Pedreschi, M. Sozzi

INFN, Sezione di Pisa, Pisa, Italy
C. Cerri, R. Fantechi, L. Pontisso [20], F. Spinella

Scuola Normale Superiore e INFN, Sezione di Pisa, Pisa, Italy
I. Mannelli

Dipartimento di Fisica, Sapienza Università di Roma e INFN, Sezione di Roma I, Roma, Italy
G. D'Agostini, M. Raggi

INFN, Sezione di Roma I, Roma, Italy
A. Biagioni, P. Cretaro, O. Frezza, E. Leonardi, A. Lonardo, M. Turisini, P. Valente, P. Vicini

INFN, Sezione di Roma Tor Vergata, Roma, Italy
R. Ammendola, V. Bonaiuto [21], A. Fucci, A. Salamon, F. Sargeni [22]

Dipartimento di Fisica dell'Università e INFN, Sezione di Torino, Torino, Italy
R. Arcidiacono [23], B. Bloch-Devaux, M. Boretto [9], E. Menichetti, E. Migliore, D. Soldi

INFN, Sezione di Torino, Torino, Italy
C. Biino, A. Filippi, F. Marchetto

Instituto de Física, Universidad Autónoma de San Luis Potosí, San Luis Potosí, Mexico
A. Briano Olvera, J. Engelfried, N. Estrada-Tristan [24], M. A. Reyes Santos [24]

Horia Hulubei National Institute for R&D in Physics and Nuclear Engineering, Bucharest-Magurele, Romania
P. Boboc, A. M. Bragadireanu, S. A. Ghinescu, O. E. Hutanu

Faculty of Mathematics, Physics and Informatics, Comenius University, Bratislava, Slovakia
L. Bician [25], T. Blazek, V. Cerny, Z. Kucerova [9]

CERN, European Organization for Nuclear Research, Geneva, Switzerland
J. Bernhard, A. Ceccucci, H. Danielsson, N. De Simone [26], F. Duval, B. Döbrich [27], L. Federici, E. Gamberini, L. Gatignon [28], R. Guida, F. Hahn †, E. B. Holzer, B. Jenninger, M. Koval [25], P. Laycock [3], G. Lehmann Miotto, P. Lichard, A. Mapelli, R. Marchevski [1], K. Massri [28], M. Noy, V. Palladino, M. Perrin-Terrin [29, 30], J. Pinzino [31], V. Ryjov, S. Schuchmann, S. Venditti

School of Physics and Astronomy, University of Birmingham, Birmingham, United Kingdom
T. Bache, M. B. Brunetti [32], V. Duk [5], V. Fascianelli [33], J. R. Fry, F. Gonnella, E. Goudzovski, J. Henshaw, L. Iacobuzio, C. Lazzeroni, N. Lurkin [8], F. Newson, C. Parkinson, A. Romano, J. Sanders, A. Sergi [34], A. Sturgess, J. Swallow [9], A. Tomczak

School of Physics, University of Bristol, Bristol, United Kingdom
H. Heath, R. Page, S. Trilov

School of Physics and Astronomy, University of Glasgow, Glasgow, United Kingdom
B. Angelucci, D. Britton, C. Graham, D. Protopopescu

Faculty of Science and Technology, University of Lancaster, Lancaster, United Kingdom
J. Carmignani [35], J. B. Dainton, R. W. L. Jones, G. Ruggiero [36]

School of Physical Sciences, University of Liverpool, Liverpool, United Kingdom
L. Fulton, D. Hutchcroft, E. Maurice [37], B. Wrona

Physics and Astronomy Department, George Mason University, Fairfax, Virginia, USA
A. Conovaloff, P. Cooper, D. Coward [38], P. Rubin

Authors affiliated with an Institute or an international laboratory covered by a cooperation agreement with CERN
A. Baeva, D. Baigarashev [39], D. Emelyanov, T. Enik, V. Falaleev [5], S. Fedotov, K. Gorshanov, E. Gushchin, V. Kekelidze, D. Kereibay, S. Kholodenko, A. Khotyantsev, A. Korotkova, Y. Kudenko, V. Kurochka, V. Kurshetsov, L. Litov [16], D. Madigozhin [*], M. Medvedeva, A. Mefodev, M. Misheva [40], N. Molokanova, S. Movchan, V. Obraztsov, A. Okhotnikov, A. Ostankov [†], I. Polenkevich, Yu. Potrebenikov, A. Sadovskiy, V. Semenov [†], S. Shkarovskiy, V. Sugonyaev, O. Yushchenko, A. Zinchenko [†]

[*]Corresponding author: F. Brizioli, D. Madigozhin,
email: francesco.brizioli@cern.ch, dmitry.madigozhin@cern.ch
[†]Deceased
[1]Present address: Ecole Polytechnique Fédérale Lausanne, CH-1015 Lausanne, Switzerland
[2]Present address: Syracuse University, Syracuse, NY 13244, USA
[3]Present address: Brookhaven National Laboratory, Upton, NY 11973, USA
[4]Present address: School of Physics and Astronomy, University of Birmingham, Birmingham, B15 2TT, UK
[5]Present address: INFN, Sezione di Perugia, I-06100 Perugia, Italy
[6]Also at TRIUMF, Vancouver, British Columbia, V6T 2A3, Canada
[7]Present address: Department of Astronomy and Theoretical Physics, Lund University, Lund, SE 223-62, Sweden
[8]Present address: Université Catholique de Louvain, B-1348 Louvain-La-Neuve, Belgium
[9]Present address: CERN, European Organization for Nuclear Research, CH-1211 Geneva 23, Switzerland

[10]Present address: Institut für Kernphysik and Helmholtz Institute Mainz, Universität Mainz, Mainz, D-55099, Germany
[11]Present address: Universität Würzburg, D-97070 Würzburg, Germany
[12]Present address: European XFEL GmbH, D-22761 Hamburg, Germany
[13]Present address: School of Physics and Astronomy, University of Glasgow, Glasgow, G12 8QQ, UK
[14]Present address: Institut für Physik and PRISMA Cluster of Excellence, Universität Mainz, D-55099 Mainz, Germany
[15]Also at Dipartimento di Scienze Fisiche, Informatiche e Matematiche, Università di Modena e Reggio Emilia, I-41125 Modena, Italy
[16]Also at Faculty of Physics, University of Sofia, BG-1164 Sofia, Bulgaria
[17]Present address: Scuola Superiore Meridionale e INFN, Sezione di Napoli, I-80138 Napoli, Italy
[18]Present address: Instituto de Física, Universidad Autónoma de San Luis Potosí, 78240 San Luis Potosí, Mexico
[19]Present address: Institut am Fachbereich Informatik und Mathematik, Goethe Universität, D-60323 Frankfurt am Main, Germany
[20]Present address: INFN, Sezione di Roma I, I-00185 Roma, Italy
[21]Also at Department of Industrial Engineering, University of Roma Tor Vergata, I-00173 Roma, Italy
[22]Also at Department of Electronic Engineering, University of Roma Tor Vergata, I-00173 Roma, Italy
[23]Also at Università degli Studi del Piemonte Orientale, I-13100 Vercelli, Italy
[24]Also at Universidad de Guanajuato, 36000 Guanajuato, Mexico
[25]Present address: Charles University, 116 36 Prague 1, Czech Republic
[26]Present address: DESY, D-15738 Zeuthen, Germany
[27]Present address: Max-Planck-Institut für Physik (Werner-Heisenberg-Institut), München, D-80805, Germany
[28]Present address: Faculty of Science and Technology, University of Lancaster, Lancaster, LA1 4YW, UK
[29]Present address: Aix Marseille University, CNRS/IN2P3, CPPM, F-13288, Marseille, France
[30]Also at Université Catholique de Louvain, B-1348 Louvain-La-Neuve, Belgium
[31]Present address: INFN, Sezione di Pisa, I-56100 Pisa, Italy
[32]Present address: Department of Physics, University of Warwick, Coventry, CV4 7AL, UK
[33]Present address: Center for theoretical neuroscience, Columbia University, New York, NY 10027, USA
[34]Present address: Dipartimento di Fisica dell'Università e INFN, Sezione di Genova, I-16146 Genova, Italy
[35]Present address: School of Physical Sciences, University of Liverpool, Liverpool, L69 7ZE, UK
[36]Present address: Dipartimento di Fisica e Astronomia dell'Università e INFN, Sezione di Firenze, I-50019 Sesto Fiorentino, Italy
[37]Present address: Laboratoire Leprince Ringuet, F-91120 Palaiseau, France
[38]Also at SLAC National Accelerator Laboratory, Stanford University, Menlo Park, CA 94025, USA
[39]Also at L.N. Gumilyov Eurasian National University, 010000 Nur-Sultan, Kazakhstan
[40]Present address: Institute of Nuclear Research and Nuclear Energy of Bulgarian Academy of Science (INRNE-BAS), BG-1784 Sofia, Bulgaria